Electronic structure of oxygen vacancies in SrTiO_{3} and LaAlO_{3}

C. Mitra, C. Lin, J. Robertson, and Alexander A. Demkov

Phys. Rev. B **86**, 155105 — Published 2 October 2012

DOI: 10.1103/PhysRevB.86.155105

Electronic structure of oxygen vacancies in $SrTiO_3$ and $LaAlO_3$

C. Mitra[a], C. Lin[a], J. Robertson[b], and Alexander A. Demkov[a1]
[a]Department of Physics, The University of Texas at Austin, Austin, TX 78712, USA
[b]Engineering Department, Cambridge University, Cambridge CB2 1PZ, UK

Abstract
The electronic structure of oxygen vacancies in bulk perovskite oxides $SrTiO_3$ and $LaAlO_3$ is studied using the Heyd, Scuseria, Ernzerhof (HSE) hybrid density functional. In $SrTiO_3$ the oxygen vacancy defect introduces a localized state comprised of $3d_{z^2}$ and $4p_z$ orbitals of the adjacent Ti atoms. This results in a bound state 0.7 eV below the conduction band edge. For $LaAlO_3$, the oxygen vacancy creates a deep state 2.19 eV below the conduction band edge. The defect state is a hybrid of the adjacent La 5*d* and the Al 3*p* states. We compute the formation energies of the neutral oxygen vacancy defect, V^0 in bulk $SrTiO_3$ and $LaAlO_3$ to be 6.0 eV and 8.3 eV, respectively.

I. Introduction

Perovskite oxides ABO_3 are widely studied as functional materials exhibiting superconductivity [1], ferroelectricity [2], magnetism [3] and a wide range of dielectric properties. Recently, $SrTiO_3$ (STO) and $LaAlO_3$ (LAO) have attracted considerable attention due to the two dimensional electron gas (2DEG) observed at the interface between these two wide gap insulators [4-13]. The origin of this 2DEG has been a source of considerable debate. Oxygen vacancies form an n-type defect in both STO and LAO and the origin of charge in LAO/STO heterostructures is sometimes attributes to the presence of these defects [14,15]. Hence, the electronic structure and nature of a vacancy induced defect states in these oxides are important.

Although the electronic structure of oxygen vacancies in STO and LAO has been studied previously with density functional theory (DFT), there are discrepancies in the literature. For STO, which has a band gap of 3.2 eV [16], it has been reported that the presence of oxygen vacancies causes strong atomic relaxation of the atoms surrounding the vacancy site, thus reducing the octahedral symmetry of the crystal to tetragonal [17]. While Louie et al. [17] found the neutral oxygen vacancy defect state to lie 0.4 eV higher than the conduction band minima, Ricci et al. [18] found the impurity state within the band gap. Kotomin et al. [19] also found a defect related gap state. The discrepancy in the results could be attributed to the different density functionals used in the calculations which yields different results for the bulk properties, to begin with. In yet another study by Buban *et al.* [20], the defect state character is found to change from a deep to a shallow (within the LDA) when the supercell size is changed from 40 to 160 atoms. While the 40 atom supercell is too small to allow for the defect induced structural relaxations, the charge density plot for their 320 atom supercell clearly shows the t_{2g} like character of the state occupied in a defect containing supercell. This is similar to our LDA calculations (see FIG.

[1] E-mail: demkov@physics.utexas.edu

4). As reported in [18], who perform oxygen vacancy calculations on STO employing a variety of functionals, the band gap within DFT-B3LYP, for instance, in bulk STO is overestimated by as much as 1.2 eV when compared to the experimental value. DFT-LDA and DFT-PW91, on the other hand underestimates it while HF severely overestimates the band gap.

Therefore, a more reliable approach is needed. The goal of this paper is to study oxygen vacancy defects in bulk LAO and STO, and determine the energy of defect levels using the Heyd, Scuseria, and Ernzerhof (HSE) hybrid density functional [21]. The reliability of HSE in computing physical properties for bulk STO has already been established before [22], which does not only refer to band gaps but also dielectric properties and the equilibrium volume. Other hybrid functional such as the B3LYP has been found to increase the equilibrium volume [22]. This incorrect behavior has been attributed to the incorrect behavior of the LYP correlation energy [22]. Although, the reliability of the HSE functional in computing defect formation energies would ultimately be have to be established by solid experimental results, it certainly seems an appropriate choice for defect study given its reasonable findings of bulk physical properties in the present materials of interest. Quasiparticle GW calculations [23], would probably be useful in this respect but they would be computationally demanding, particularly for a defect study.

An important aspect of the difference between the two materials lies in the nature of the conduction band edge. While in STO it is comprised mainly of Ti 3*d* states, in LAO it is formed of the La 5*d* states. This, combined with the difference in location of these atomic sites in the crystal lattice, results in an important difference in the nature of the vacancy-related defect state in two materials. Having determined the electronic structure of the defects, we compute the formation energy of both the neutral and charged (V^{+}, V^{++}, V^{-} and V^{--}) vacancies as a function of the Fermi energy. The reference oxygen chemical potential, chosen for all the above calculations is half the energy of an isolated oxygen molecule [24].

The paper is organized as follows. In sec. II we briefly described computational methodologies used. Sec. III presents the results and discussions followed by sec IV which draws the conclusions.

II. Computational methods

In the HSE formalism [21], the exchange correlation functional is constructed from 25 % Hartree-Fock exchange (E_x) and 75% of the generalized gradient approximation due to Perdew, Burke and Ernzerhof (PBE) [25]. The method has an advantage over the PBEh [26,27] hybrid functional due to its faster convergence. This is because in HSE the exact exchange is further decomposed into a long range and a short range part in real space. The range separation is determined by a parameter, μ, which is typically chosen as a distance at which the non-local long range interaction becomes negligible. The HSE exchange correlation functional is written as:

$$E_{xc}^{HSE} = \frac{1}{4} E_x^{sr,\mu} + \frac{3}{4} E_x^{PBE,sr,\mu} + E_x^{PBE,lr,\mu} + E_c^{PBE} \qquad (1)$$

where the superscript sr and lr stand for short range and long range, respectively, and μ is the screening parameter mentioned earlier.

All calculations are done using the Vienna Ab-initio Simulation Package (VASP) code [28] with the HSE implementation described in [29]. We use projector augmented wave pseudopotentials [30] for both STO and LAO. For La, $5s^2\ 5p^6\ 5d^1\ 6s^2$ are included as valence electrons. For Sr and Ti, $3s^2\ 3p^6\ 4s^2$ and $3s^2\ 3p^6\ 4s^2\ 3d^2$ are included, respectively. We use μ values of 0.3 $Å^{-1}$ for STO [22] and 0.2 $Å^{-1}$ for LAO in order to reproduce the experimental band gap. It is important to note that although μ affects band gaps it does not influence the total energy [22,31,32]. A plane wave cut off energy of 600 eV is used and a 6x6x6 Monkhorst-Pack special k-point grid [33] for bulk and 4x4x2 for the supercell are chosen for integration over the Brillouin zone. The energies are converged to within 10^{-6} eV/cell. All forces are converged to within 0.004 eV/Å.

III. Results and Discussion

Bulk density of states with HSE

At room temperature STO has a cubic perovskite ($Pm\bar{3}m$) crystal structure while LAO has a rhombohedral perovskite ($R\bar{3}c$) structure. The HSE band gaps and the lattice parameters of STO and LAO are compared to the LDA values in Tables 1 and 2, respectively. The HSE band gaps of 3.01 eV and 5.0 eV for STO and LAO, respectively, are in good agreement with experiment [16,34], and show a considerable improvement over the LDA band gaps. In FIGS. 1 and 2 we show the partial density of states (PDOS) for bulk STO and LAO, respectively. The valence band edge in both oxides is comprised mainly of the oxygen *p* states. We would like point out two important observations here. First, while the conduction band minima of both STO and LAO are composed of the *d* states, in STO they are mainly the Ti *3d* t_{2g} states and in LAO they are the La *5d* e_g states. Second, using HSE, the separation between e_g and t_{2g} bands of STO is reduced by roughly 1 eV as compared to that in LDA. As we will show, these differences of the electronic structure have a profound effect on the character of the oxygen vacancy state.

Modeling an oxygen vacancy

$SrTiO_3$

In order to model a point defect in cubic STO we build a 2x2x4, 80 atom supercell and create an oxygen vacancy as shown in FIG. 3. Introduction of a neutral oxygen vacancy causes large structural relaxation of the atoms around the vacancy site. Local structural changes are distinctly different when we compare the LDA and HSE calculations. This in turn affects the electronic structure of the defect state within the two levels of theory. Within the LDA, the neighboring Ti atoms (marked A and B in FIG. 3) move away from each other by 0.3 Å, similar to the results

reported in [17]. However, this is opposite to what happens within HSE where the two Ti atoms, in fact, move closer to each other by 0.12 Å. We note that similar effects were found with the HF-DFT hybrid approach [35]. In order to understand these structural relaxations, we examine the defect PDOS.

An oxygen vacancy donates two electrons to the system and leads to the formation of two dangling bonds on the neighboring Ti atoms. It also reduces the octahedral (O_h) symmetry of the neighboring Ti atoms to a tetragonal (C_{4v}) symmetry. This in turn leads to a local hybridization of the Ti $3d_z^2$, the 4*p* and the 4*s* states, of which the defect state is now comprised. This hybridization plays an important role in creating a localized defect bound state. A detailed quantitative analysis employing tight-binding calculations will be discussed elsewhere [36]. The neighboring Sr atoms do not contribute to the defect state as the unoccupied Sr states lie much higher in the conduction band than the Ti *d* states. Hence we specifically project out the Ti states of the atom marked 'A' in FIG. 3.

As seen in FIG. 4, within the LDA we do not find a defect state in the band gap, the bottom of the conduction band has a t_{2g} character, and the system is metallic. The $3d_z^2$ e_g states on Ti atoms adjacent to the vacancy (z-axis coincides with Ti-vacancy-Ti line) form a bonding/anti-bonding pair. Note, that the *p-d* mixing manifests itself in a large 2 eV splitting between the bonding and anti-bonding defect states. However, the defect bonding state ($3d_z^2$ e_g) is a band resonance. The $3d_{x^2-y^2}$ e_g state lies even higher in the band. Within the LDA one could say that the backbone Ti-oxygen atoms win, and Ti atoms relax away from the vacancy leaving the empty bonding defect state above the band edge.

In order to alleviate the uncertainty of the defect level position with respect to the band edge, it is interesting to go beyond the LDA. One option is to use the Hubbard correction in the LDA+U formalism [37]. The band gap is certainly improved, but it is not clear that the right physics is captured since the d-band is not highly correlated. However, as we have shown above, HSE gives STO and LAO band gaps in close agreement with experiment and since it partially solves the self-interaction problem, it is a natural choice for a localized defect state study.

Upon relaxing the defect-containing supercell using HSE, we find that the Ti atoms A and B are no longer pushed apart but in fact move closer to each other. The bonding state now appears as the occupied defect level lying 0.7 eV below the conduction band edge and the anti-bonding state is a band resonance. Again, the large splitting between the bonding and the anti-bonding states is due to local hybridization of the Ti $3d_z^2$, the 4*p* and the 4*s* states, which in turn leads to a large overlap between the two Ti orbitals. The orbital-decomposed DOS of the defect state is shown in FIG. 5. Several effects contribute to pushing the defect level below the band edge. Since the overlap between the Ti orbitals increases slightly, the bonding/anti-bonding splitting thereby increases from 2 eV to 2.2 eV (FIG. 4 and 5) and the average position of the defect state moves further down with respect to the t_{2g} manifold. The latter is due to the partial removal of the self-interaction, which affects localized nature of the e_g like defect state shown in FIG. 5. It is curious

to compare the HSE result with that obtained using the Hubbard correction to the LDA. While results obtained using U of 8.0 eV for Ti *3d* states [38] are identical to those obtained with HSE the reason is different. In the Hubbard model the unoccupied state is pushed up while in HSE the occupied narrow band is pushed down, both resulting in the reduction of the e_g-t_{2g} splitting.

The opposite relaxations using HSE and LDA may be understood in the following way. If the in-gap bound state already exists in the *un-relaxed* calculation (HSE and LDA+U cases), and two electrons due to OV are localized in such a state, then upon relaxation two Ti atoms would gain energy by moving closer to each other. This however, is counterbalanced by the backbone interaction with oxygen. Should it be stronger, Ti atoms would relax outwards. If no in-gap bound state exists in the un-relaxed calculation (LDA case), and two electrons due to OV are at the bottom of t_{2g} bands, bringing Ti atoms closer to each other doesn't gain energy for these two electrons but would raise the energy of the backbone. Therefore, upon relaxation Ti atoms are pushed apart to gain energy from bonding with oxygen. As pointed out earlier, within HSE the separation between e_g and t_{2g} bands is 1 eV less than that obtained in the LDA. And the bound state (formed from the e_g states) exists in HSE even before relaxation. It still may have disappeared if Ti atoms moved outward. However, the overlap of hybridized Ti orbitals stabilizes inward relaxation. In addition, HSE removes self-interaction, which is more pronounced for localized states such as the bound state of a vacancy, thus further lowering the defect state.

Different relaxation effects within the LDA and HSE have also been observed for a vacancy in rutile TiO_2 by Janotti *et. al.* [39], and it is interesting to compare with their results. Similar to our findings, in [39] the HSE functional leads to a larger bulk gap in TiO_2 and different lattice relaxation in the presence of an oxygen vacancy as compared to the LDA. The outward relaxation is significantly reduced within HSE. In STO we find HSE relaxation *opposite* to that obtained with the LDA. There are several differences between rutile TiO_2 and STO. First, in rutile the bound state due to the oxygen vacancy already *exists for the un-relaxed geometry* in both LDA and HSE. The outward relaxation of Ti in LDA removes the bound state, but preserves it in HSE due to a higher energy of the conduction band edge. In STO the bound state doesn't exist in the un-relaxed LDA, but appears within HSE as the band gap opens. Second, in STO the bonding/anti-bonding splitting of the defect state is large and sensitive to relaxation due to the highly directional character of the orbitals (the e_g orbitals point along the vacancy line). In other words the gain of lowering the bound state is larger than reaction of the backbone.

Upon removing an electron from the vacancy site, it becomes positively charged (V^{+}). This pushes the cations away from the vacancy and attracts the anions. Hence the Ti atoms relax outward away from the vacancy thus strengthening the bonding with backbone oxygen. This effect is further enhanced for the V^{++} charged state as the Ti atoms move further apart. This is also reflected in the electronic structure as the charged defect states are pushed closer to the conduction band edge because the Ti-Ti bonding becomes weaker. The position of the defect

levels of V^0, V^+ and V^{++} in STO, with respect to the valence band maximum (VBM) and conduction band minimum (CBM) are summarized in FIG. 6.

$LaAlO_3$

A similar procedure, as in STO, is adopted in order to model the oxygen vacancy defect in LAO. A 2x2x2 supercell (80 atoms) is constructed with an oxygen vacancy in it. In LAO we find the neutral vacancy defect state to lie inside the band gap both within LDA and HSE. HSE further opens up the band gap placing the V^0 level at 2.19 eV below the conduction band edge (it is 1.32 eV in the LDA). Our results differ from that reported in [40] where the defect state is found to be less deep. Discrepancies could arise due to the different supercell size used. Further, the band gap obtained with screened exchange in [40] for bulk LAO, is 4.4 eV compared to 5.0 eV obtained with HSE.

The vacancy site in LAO is surrounded by four neighboring La atoms and two Al atoms. The orbital decomposed DOS (FIG. 7(a) and (b)) of the defect state shows that it is mainly comprised of the La d_{xy} and the d_z^2 orbitals as well as the Al p orbitals. The reduced symmetry of the La atoms adjacent to the vacancy site allows local hybridization of the La d_{xy} and the d_z^2 states and hence contributes to the defect state. The Al p states (more specifically the p_z states) are directly oriented towards the vacancy (forming a σ like bond similar to the Ti atoms in STO) and hence also have a strong contribution to the defect state.

For the V^+ and V^{++} charged states we find an outward relaxation of cations, both Al and La atoms. The neutral and charged defect levels in LAO, computed with respect to the band edges, are summarized in FIG. 8.

Since the neutral oxygen vacancy defect in LAO is a deep defect we further check the presence of V^- and V^{--} state inside the gap. We do not find any states occurring within the band gap of LAO corresponding to the above charged states. The extra electrons occupy the conduction bands instead.

An interesting aspect that comes out from the above calculations is that upon aligning the bulk bands of both STO and LAO [7], charge transfer could take place from the V^+ state of LAO to either the conduction band or to the V^+ state of STO, which lies 1.19 eV below that of LAO. However, this is simply an estimate made from bulk calculations which does not take into account the various complicated mechanisms that occurs at the LAO/STO interface.

Formation energies

The formation energies of the V^0, V^+ and V^{++} defects are computed using the Zhang-Northrup formalism described in [41]:

$$\Delta H_{D,q}(E_F,\mu) = [E_{D,q} - E_H] + \sum_\alpha n_\alpha \mu_\alpha + qE_F \qquad (2)$$

The first two terms in the square brackets on the right hand side of eq. 2 are the total energies of the supercell with and without the defect, and q denotes the charge state of the system. μ_α is the chemical potential of the atoms added ($n_\alpha = -1$) or removed ($n_\alpha = +1$) from the crystal while forming the defect and E_F is the Fermi energy. Hence E_F varies between the VBM and CBM.

It is important to examine the errors that could arise due to finite supercells that are used to simulate defects in the dilute limit. However, various correction schemes that are reported in literature depend critically on supercell shape and size as has been extensively studied in [42,43,44,45]. Hence formation energy calculations of larger supercells are certainly desirable, especially for charged defects. In order to see the scaling of formation energies of neutral and charged defects as a function of supercell size we have performed calculations on supercells (within LDA) containing upto 320 atoms. With HSE we have been limited to a 135 atom supercell due to its high computational cost. FIG. 11 (a) and 11 (b) represents formation energy calculations as a function of supercell size within LDA and HSE, respectively. Going from the 135 atom supercell to that containing 320 atoms, we find that the values for the neutral and +1 charged state change by less than 0.05 eV. This convergence level is in agreement to that obtained previously by Astala *et. al.* [46] where convergence checks with respect to higher k point density and supercell size had been done on oxygen vacancy defect in STO. They had employed a local spin density approximation-plane wave pseudopotential menthod. For the +2 charged state, however, we find the formation energy changed by 0.2 eV suggesting larger supercells may be needed in order to achieve a better convergence.

The formation energies, of neutral and charged oxygen vacancies in STO and LAO, computed within LDA and HSE, are presented in FIG. 9 and 10 as a function of the Fermi level position in the gap. With μ_α chosen as the energy of a half of an oxygen molecule [24], we find that in both STO and LAO the neutral oxygen vacancy has a high formation energy of 6 eV and 8.3 eV respectively, thereby suggesting that it is unlikely to form at room temperature. However, V^+ and V^{++} states have their formation energies lowered as the Fermi level is pushed down from the CBM towards the VBM. In STO the (0/+), (0/++) and (+/++) transitions occur at 0.4, 0.53 and 0.67 eV below the edge, respectively. Thus V^{++} state is the most stable one within most of the Fermi level position range. Note that our formation energies for neutral and charged oxygen vacancies in STO differ from those obtained by Tanaka *et. al.* [47] due to the difference in the oxygen chemical potential,μ_α, chosen in [47]. In LAO the (0/++) transition occurs 1.0 eV below the band edge and V^+ is never stable. Curiously, (0/-) transition occurs right at the band edge. Overall, positively charged vacancies are likely to occur, particularly if the Fermi level is set in the lower part of the gap *e.g.*, by putting a metal contact [48]. Negatively charged vacancies are unlikely.

IV. CONCLUSIONS

In conclusion, we have performed first principles calculations for neutral and charged oxygen vacancy defects in bulk STO and LAO using the HSE functional, which shows considerable improvements in computing band gaps when compared to DFT-LDA. The defect environment is modeled with large supercells of 80 atoms for both oxides. While within the LDA there is no defect state in the gap for the V_0 state in STO, there is clearly a deep gap state 0.7 eV below the band edge within HSE. The V^+ and V^{++} states are pushed closer to the conduction band edge. In LAO, both within LDA and HSE, the oxygen vacancy is a deep state lying inside the gap. The charged states follow a trend similar to STO. Upon computing the formation energies of the above defects we find that the V^{++} state is the most stable defect for both STO and LAO. One other implication from the above oxygen vacancy defect calculations in bulk STO and LAO is that if the V^+ state could be stabilized at the LAO/STO interface charge transfer from LAO to STO would be observed.

This work is supported by the National Science Foundation under grant DMR-0548182, the US Department of Energy (DOE) under grant DE-SC0001878, and Texas Advanced Computing Center.

References

[1] C. S. Koonce, M. L. Cohen, J. F. Schooley, W. R. Hosler, and E. R. Pfeiffer, Phys. Rev. **163**, 380 (1967).

[2] Lines, M. E. & Glass, A. M. *Principles and Applications of Ferroelectrics and Related Materials* (Clarendon, Oxford, 1977).

[3] Crystallography and Chemistry of Perovskites, M. Johnsson and P. Lemmens, in "Handbook of Magnetism and Advanced Magnetic Media", H. Kronmüller (Ed.), John Wiley & Sons, New York, (2006), cond-mat/0506606.

[4] A. Ohtomo and H. Y. Hwang, Nature (London) **427**, 423 (2004).

[5] S. Thiel, G. Hammerl, A. Schmehl, C. W. Schneider, J. Mannhart, Science **313**, 1942 (2006).

[6] N. Nakagawa, H. Y. Hwang, and D. A. Muller, Nature Mat. **5**, 204 (2006).

[7] J. K. Lee and A. A. Demkov, Phys. Rev. B. **78**, 193104 (2008).

[8] R. Pentcheva and W. E. Pickett, Phys. Rev. Lett. **102**, 107602 (2009).

[9] C. L. Jia, S. B. Mi, M. Faley, U. Poppe, J. Schubert, and K. Urban, Phys. Rev. B **79**, 081405(R) (2009).

[10] Y. Segal, J. H. Ngai, J. W. Reiner, F. J. Walker, and C. H. Ahn, Phys. Rev. B **80**, 241107(R) (2009).

[11] S. A. Pauli, S. J. Leake, B. Delley, M. Björck, C. W. Schneider, C. M. Schlepütz, D.

Martoccia, S. Paetel, J. Mannhart, and P. R. Willmott, Phys. Rev. Lett. **106**, 036101 (2011).

[12] J. Mannhart and D. G. Schlom, Science **327**, 1607 (2010).

[13] H. Chen, A. M. Kolpak, and S. Ismail-Beigi, Adv. Mat. **22**, 2881 (2010).

[14] W. Siemons, G. Koster, H. Yamamoto, W.A Harrison, G. Lucovsky, T.H. Geballe, D.H.A Blank, and M.R. Beasley, Phys. Rev. Lett. **98**, 196802 (2007).

[15] A. Kalabukhov, R. Gunnarsson, J. Börjesson, E. Olsson, T. Claeson, and D. Winkler, Phys. Rev. B **75**, 121404(R) (2007).

[16] K. van Benthem and C. Elsässer, J. Appl. Phys. **90**, 6156 (2011).

[17] W. Luo, W. Duan, S. G Louie, and M. L. Cohen, Phys. Rev. B **70**, 214109 (2004).

[18] D. Ricci, G. Bano, G. Pacchioni, and F. Illas, Phys. Rev. B **68**, 224105 (2003).

[19] J. Carrasco, F. Illas, N. Lopez, E. A. Kotomin, Y. F. Zhukovskii, R. A. Evarestov, Y. A. Mastrikov, S. Piskunov, and J. Maier, Phys. Rev. B **73** 064106 (2006).

[20] J. P. Buban, H. Iddir, and S. Ogut, Phys. Rev. B **69**, 180102(R) (2004).

[21] J. Heyd, G. E. Scuseria, and M. Ernzerhof, J. Chem. Phys. **118**, 8207 (2003); **124**, 219906(E) (2006).

[22] R. Wahl, D. Vogtenhuber, and G. Kresse, Phys. Rev. B **78**, 104116 (2008).

[23] T. Kotani, M. van Schilfgaarde, S. V Faleev and A. Chantis, J. Phys.: Condens. Matter **19** 365236 (2007).

[24] R. O. Jones and O. Gunnarsson, Rev. Mod. Phys. **61**, 689 (1989).

[25] J. P. Perdew, K. Burke, and M. Ernzerhof, Phys. Rev. Lett. **77**, 3865 (1996).

[26] C. Adamo and V. Barone, J. Chem. Phys. **110**, 6158 (1999).

[27] J. P. Perdew, M. Ernzerhof, and K. Burke, J. Chem. Phys. **105**, 9982 (1996).

[28] G. Kresse and J. Furthmüller, Phys. Rev. B **54**, 11169 (1996).

[29] J. Paier, M. Marsman, K. Hummer, G. Kresse, I. C. Gerber, and J. G. Ángyán, J. Chem. Phys. **124**, 154709 (2006); **125**, 249901(E) (2006).

[30] P. E. Blöchl, Phys. Rev. B **50**, 17953 (1994).

[31] A. I. Lebedev, Phys. Solid State **51**, 362 (2009).

[32] A. R. Akbarzadeh, I. Kornev, C. Malibert, L. Bellaiche, and J. M. Kiat, Phys. Rev. B **72**, 205104 (2005).

[33] H. J. Monkhorst and J. D. Pack. Phys. Rev. B **13**, 5188 (1976).

[34] S. G. Lim, S. Kriventsov, T. N. Jackson, J. H. Haeni, D. G. Schlom, A. M. Balbashov, R. Uecker, P. Reiche, J. L. Freeouf, and G. Lucovsky, J. Appl. Phys. **91**, 4500 (2002).

[35] V.E Alexandrov, E.A Kotomin, J. Maier, and R.A. Evarestov, Eur. Phys. J. **B** 72, 53-57 (2009).

[36] C. Lin, C. Mitra, and A. A. Demkov, submitted (2012).

[37] S. L. Dudarev, G. A. Botton, S. Y. Savrasov, C. J. Humphreys, and A. P. Sutton, Phys. Rev. B **57**, 1505 (1998).

[38] This large value of U results in the experimental band gap of STO as has been shown in [7].

[39] A. Janotti, J. B. Varley, P. Rinke, N. Umezawa, G. Kresse, and C. G. Van de Walle, Phys. Rev. B **81**, 085212 (2010).

[40] K. Xiong, J. Robertson, and S. J. Clark, Appl. Phys. Lett. **89**, 022907 (2006).

[41] S. B. Zhang and J. E. Northrup, Phys. Rev. Lett. **67**, 2339 (1991).

[42] N. D. M. Hine, K. Frensch, W. M. C. Foulkes, and M. W. Finnis, Phys. Rev. B **79**, 024112 (2009).

[43] S. E. Taylor and F. Bruneval, Phys. Rev. B **84**, 075155 (2011).

[44] C. W. M. Castleton, A. Hglund, and S. Mirbt, Phys. Rev. B **73**, 035215 (2006).

[45] J. Shim, E.-K. Lee, Y. J. Lee, and R. M. Nieminen, Phys. Rev. B **71**, 035206 (2005).

[46] R. Astala and P. D. Bristowe, Modell. Simul. Mater. Sci. Eng. **9**, 415 (2001).

[47] T. Tanaka, K. Matsunaga, Y. Ikuhara, and T. Yamamoto, Phys. Rev. B **68**, 205213 (2003).

[48] A.A. Demkov, Phys. Rev. B **74,** 085310 (2006).

Tables

Table 1. Comparison of the calculated and experimental lattice constant ***a*** and band gap E_g of $SrTiO_3$

	LDA	**HSE**	**Experiment**
***a* (Å)**	3.86	3.90	3.89[a]
E_g (eV)	1.87	3.01	3.25[b]

[a]Reference [41]
[b]Reference [16]

Table 2. Comparison of calculated and experimental lattice parameters and band gap E_g of $LaAlO_3$. α refers to the rhombohedral angle and Φ refers to the octahedral tilt about the [111] direction.

	LDA	**HSE**	**Experiment**
a (Å)	5.32	5.35	5.36[a]
α (deg)	60.1	60.12	60.15[a]
Φ (deg)	6.1	6.00	5.70[a]
E_g (eV)	3.51	5.00	5.40[b]

[a]Reference [42]
[b]Reference [34]

Figure captions

FIG. 1. (Color online) (a) Orbital projected DOS (LDA) of Titanium (Ti) states in STO. (b) Orbital projected DOS (HSE) of Titanium (Ti) states in STO. (c) Orbital projected DOS (HSE) of Oxygen (O) states in STO. Zero energy is set at the top of the valence band.

FIG. 2. (Color online) (a) Orbital projected DOS (HSE) of Lanthanum (La) states in LAO. (b) Orbital projected DOS (HSE) of O states in LAO. Zero energy is set at the top of the valence band.

FIG. 3. (Color online) STO supercell containing an oxygen vacancy.

FIG. 4. (Color online) (a) LDA orbital projected DOS of Ti atom close to the vacancy site. The Fermi level is indicated by the dashed line showing the highest occupied state. Ti d_z^2 peaks (blue) around 0.8 eV and 2.8 eV correspond to the bonding and antibonding states respectively.

FIG. 5. (Color online) Orbital decomposed DOS (HSE) of a Ti atom (marked A in FIG. 2) contributing to the defect state. The Fermi level is indicated by the dashed line showing the highest occupied state. Ti d_z^2 peaks around -0.4 eV and 1.8 eV correspond to the bonding and antibonding states respectively.

FIG. 6. (Color online) Energy levels of V_0, V^+, and V^{++} in STO (HSE) with respect to VBM and CBM.

FIG. 7(a). (Color online) Contribution to the defect state (HSE) from one of the neighboring La atoms.(b). Contribution to the defect state (HSE) from one of the neighboring Al atoms.

FIG. 8. (Color online) Defect levels (HSE) in LAO

FIG. 9(a). (Color online) Formation energy of an oxygen vacancy in various charged states in STO (HSE).

FIG. 9(b). (Color online) Formation energy of an oxygen vacancy in various charged states in STO (LDA).

FIG. 10(a). (Color online) Formation energy of an oxygen vacancy in various charged states in LAO (HSE).

FIG. 10(b). (Color online) Formation energy of an oxygen vacancy in various charged states in LAO (LDA).

FIG. 11(a). (Color online) Formation energy of neutral and charged oxygen vacancy defects, in STO, as a function of supercell size (LDA). The formation energy of the charged defects shown in the plot correspond to E_F=0 eV.

FIG. 11(b). (Color online) Formation energy of neutral and charged oxygen vacancy defects, in STO, as a function of supercell size (HSE). The formation energy of the charged defects shown in the plot correspond to E_F=0 eV.

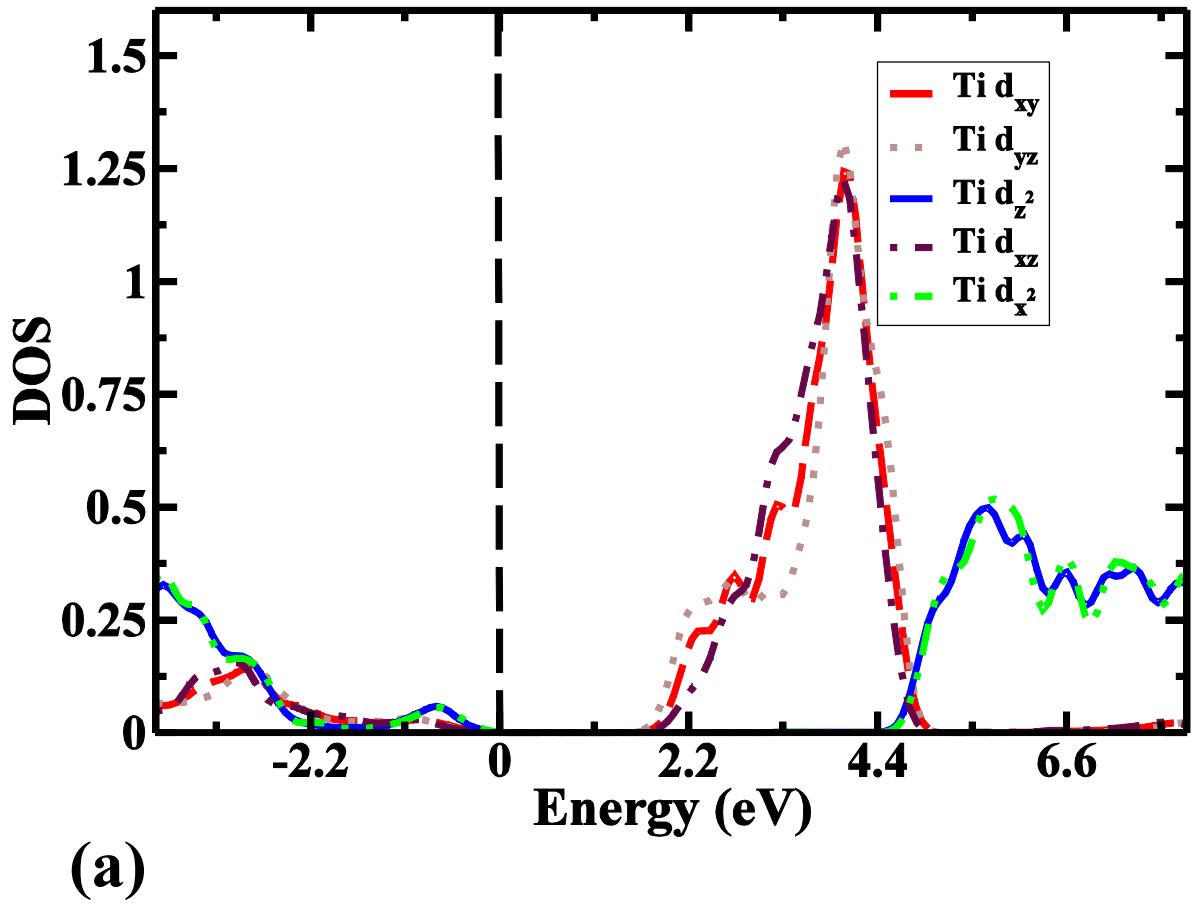

(a)

Figure 1a BL11919 19SEP2012

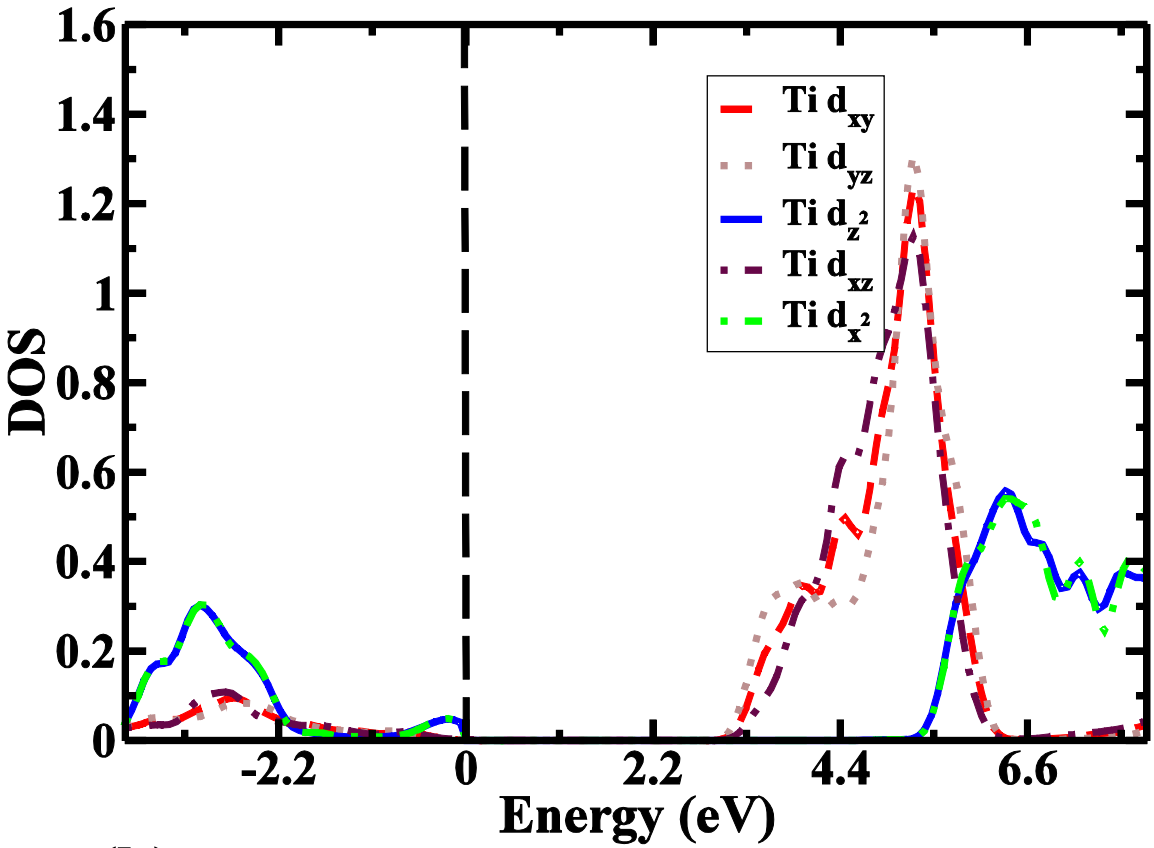

(b)

Figure 1b BL11919 19SEP2012

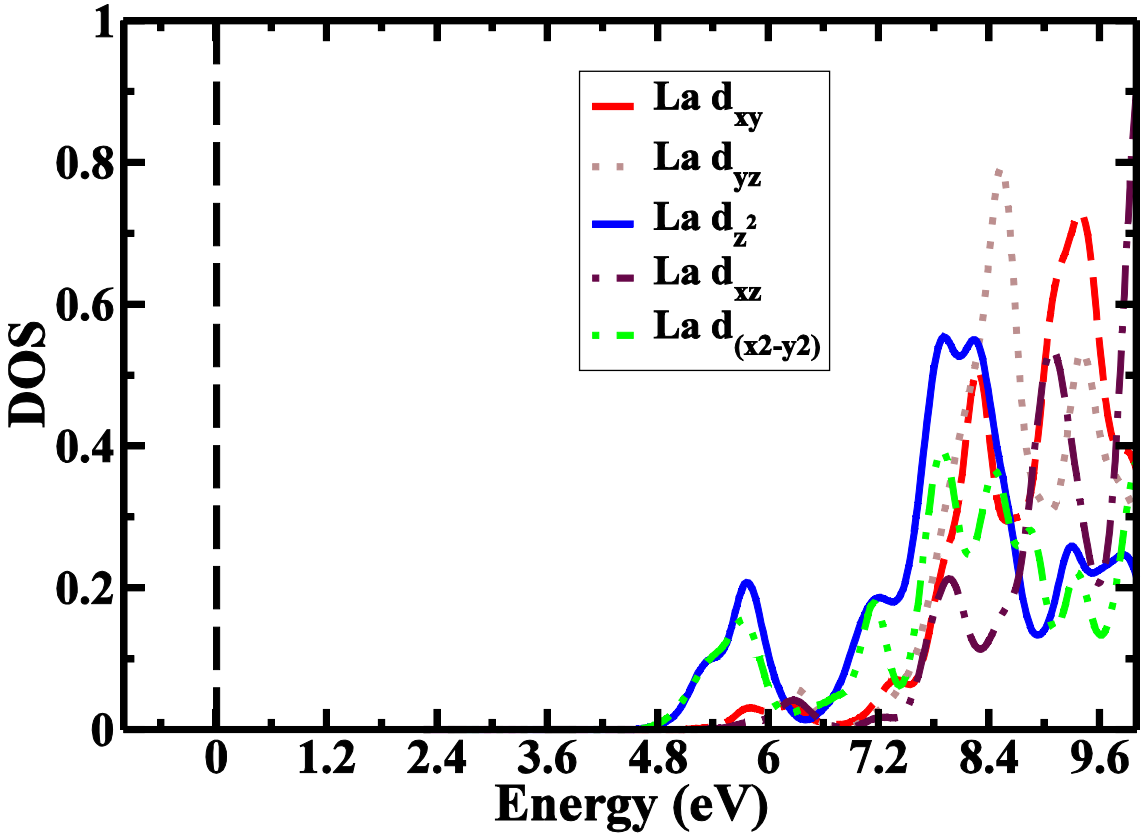

(a)

Figure 2a BL11919 19SEP2012

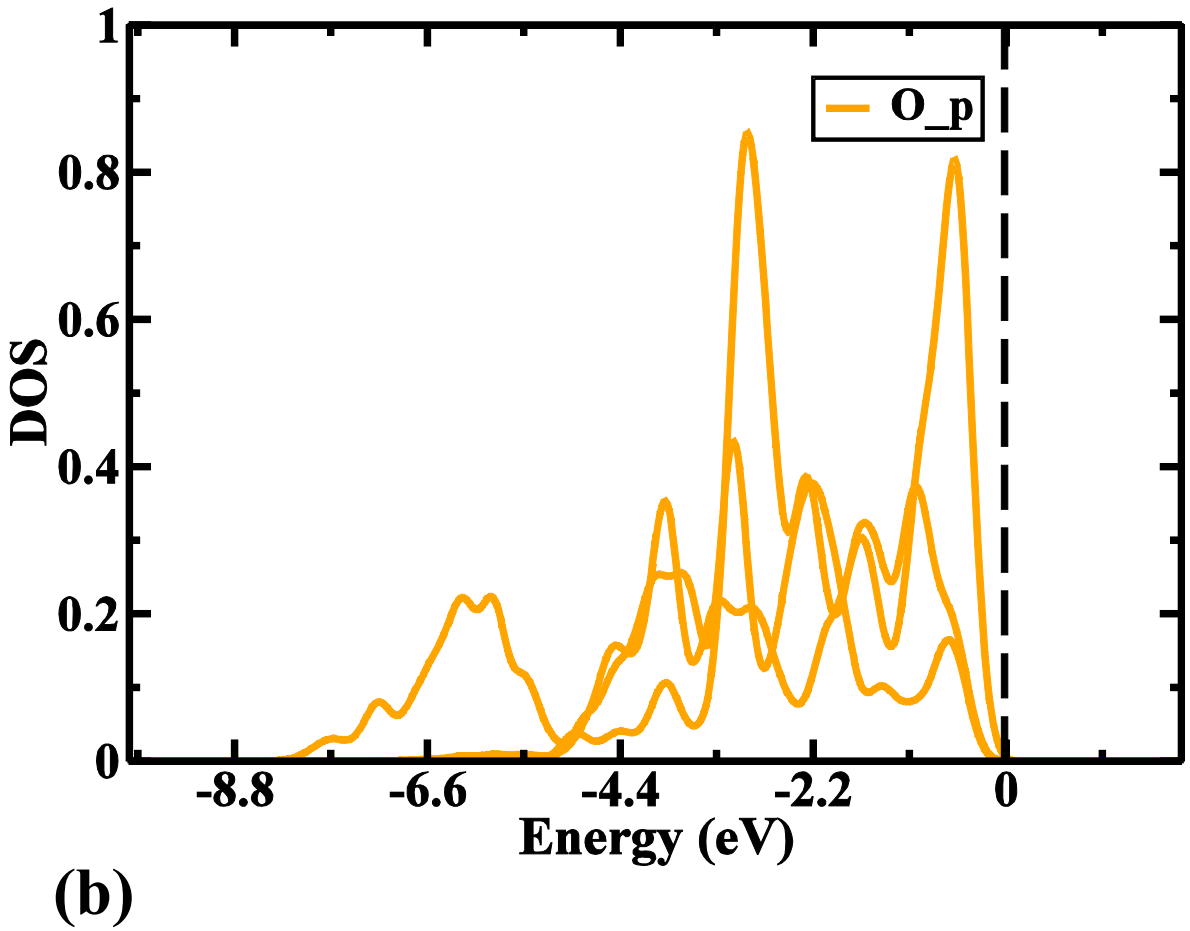

(b)

Figure 2b BL11919 19SEP2012

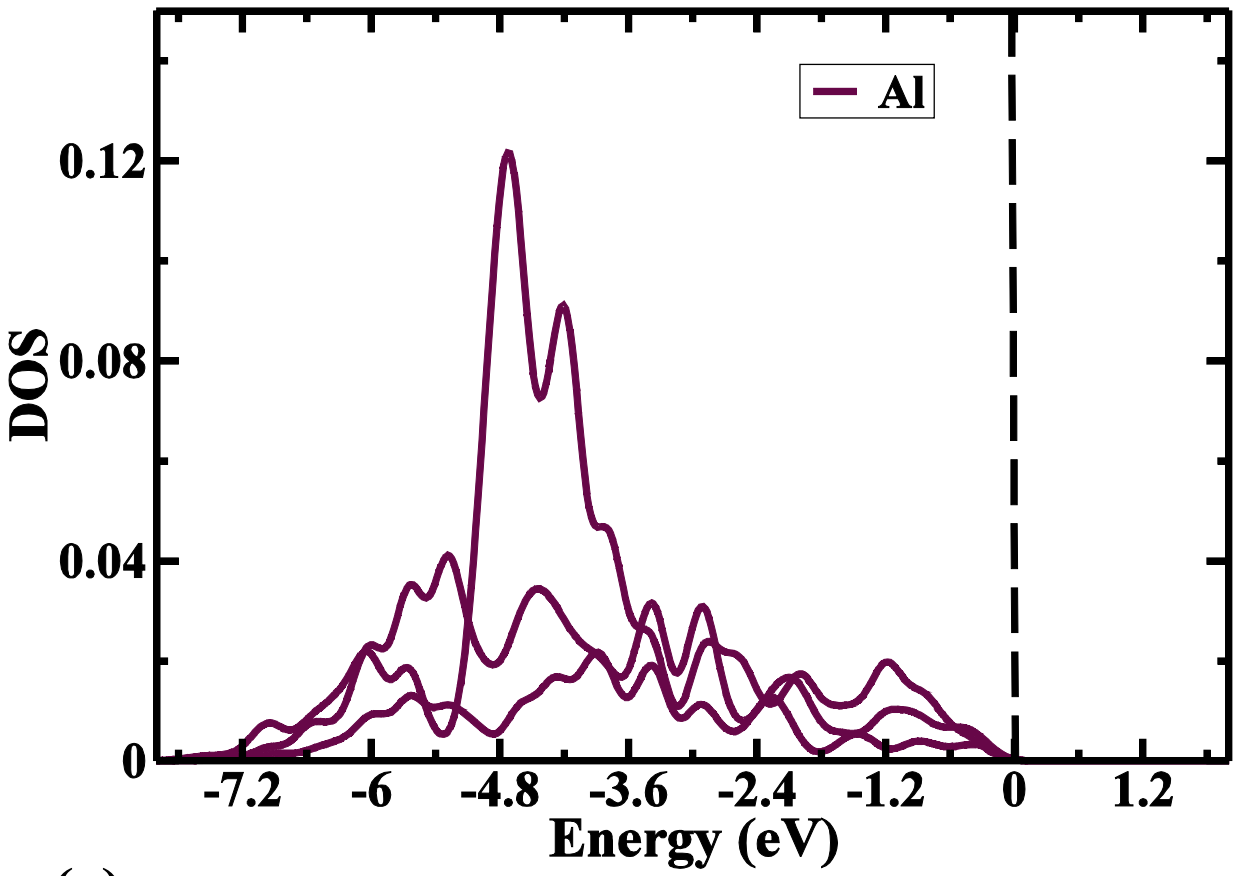

(c)

Figure 2c BL11919 19SEP2012

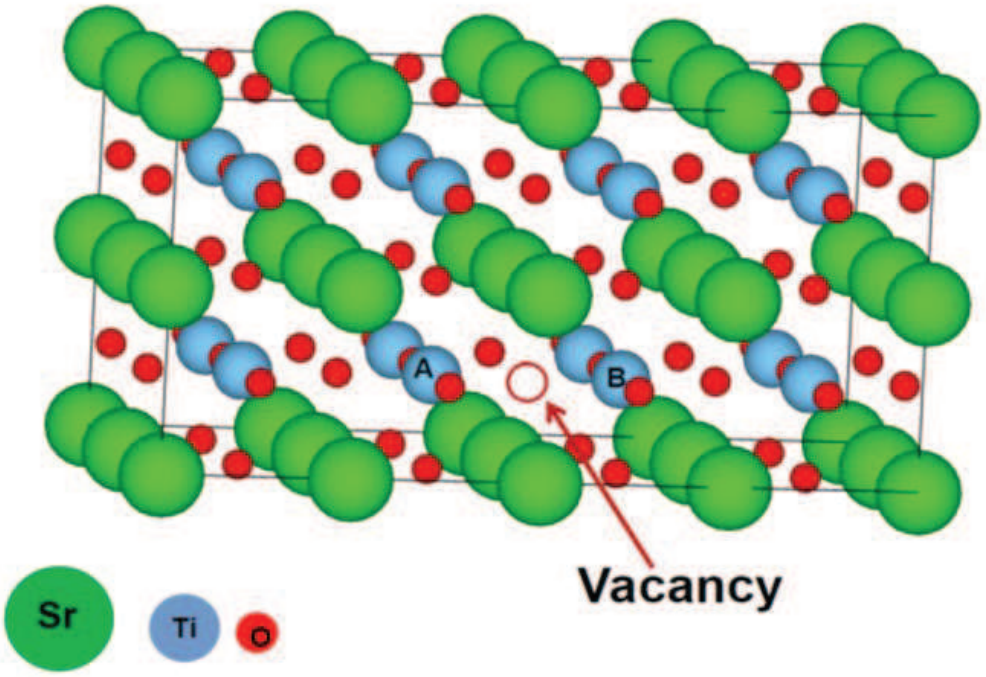

Figure 3 BL11919 19SEP2012

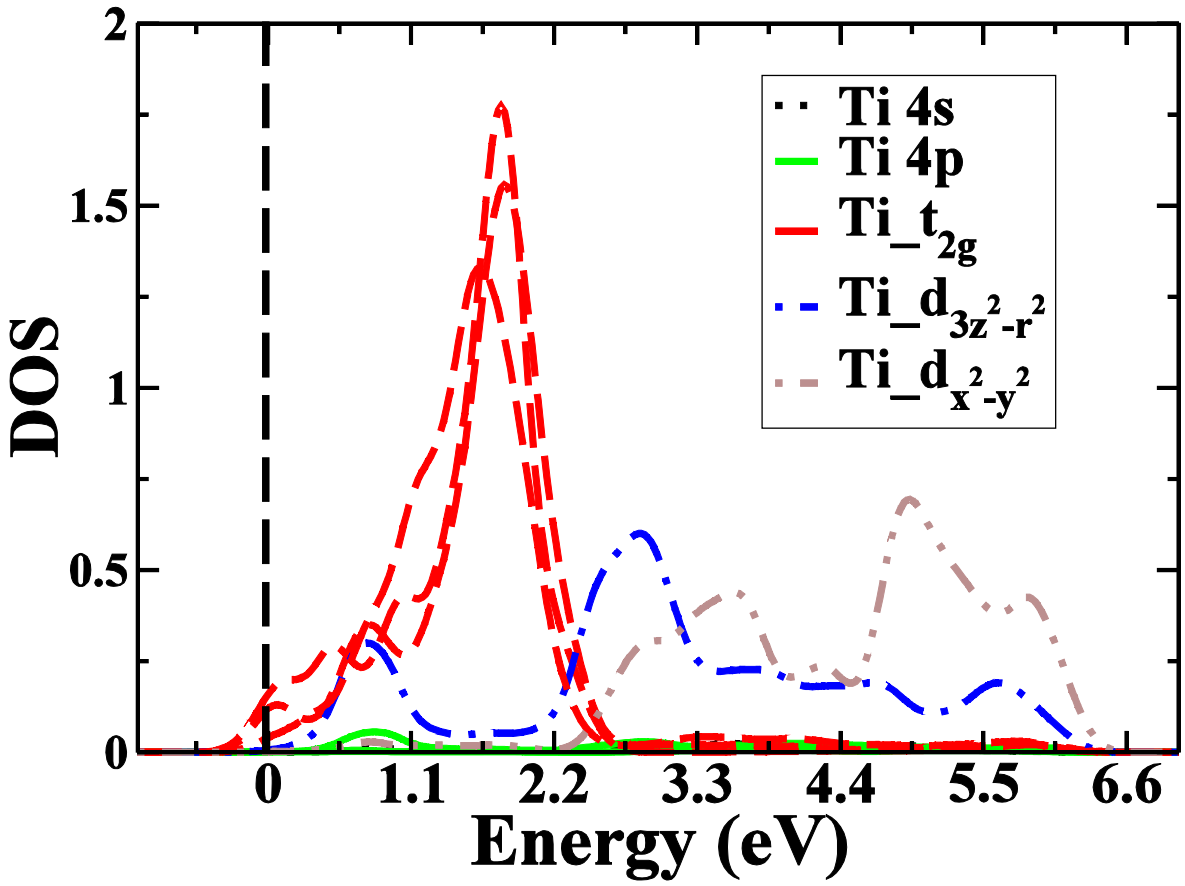

Figure 4 BL11919 19SEP2012

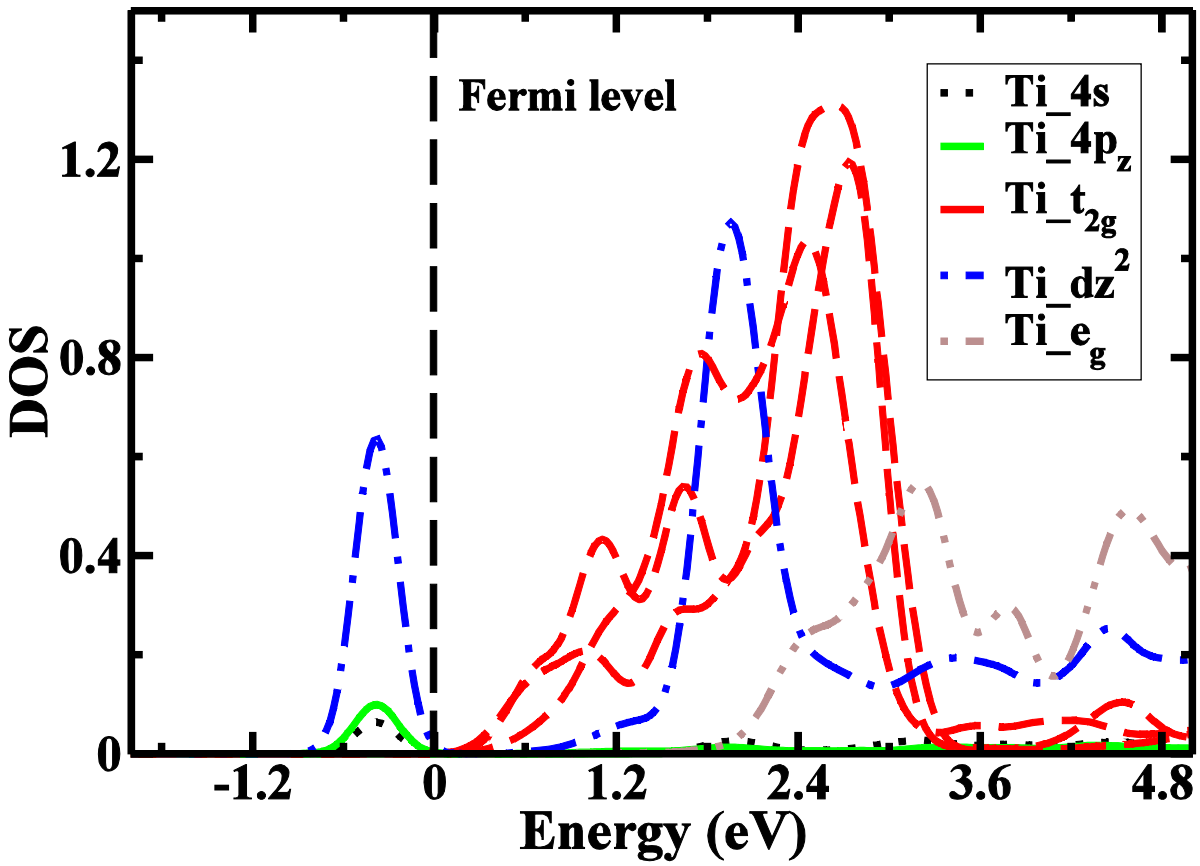

Figure 5 BL11919 19SEP2012

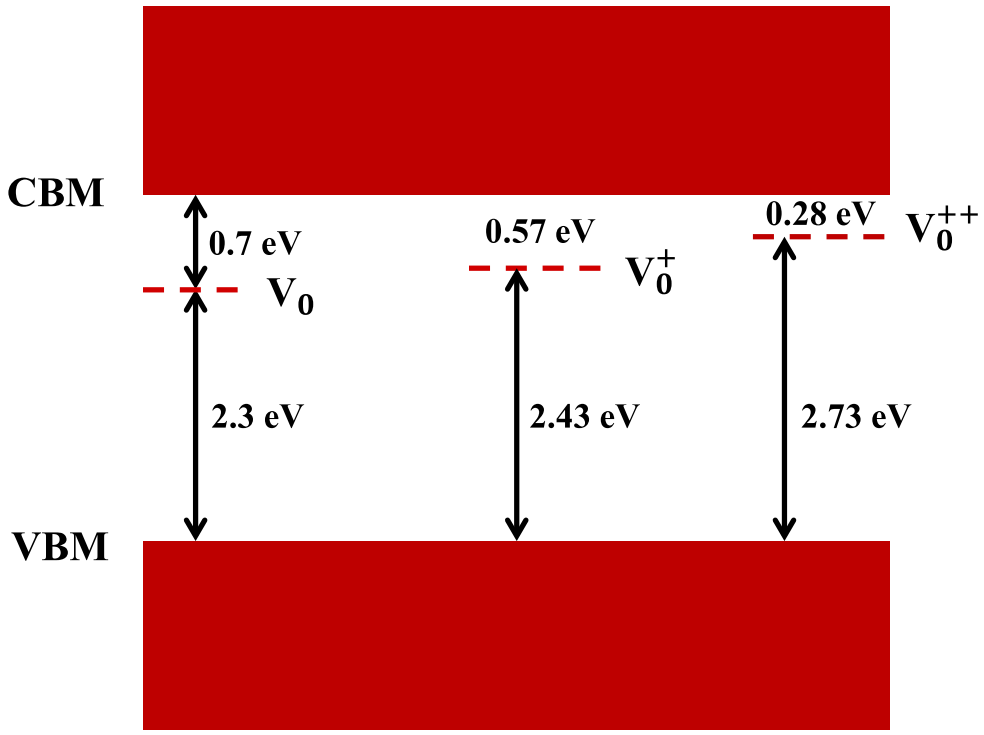

Figure 6 BL11919 19SEP2012

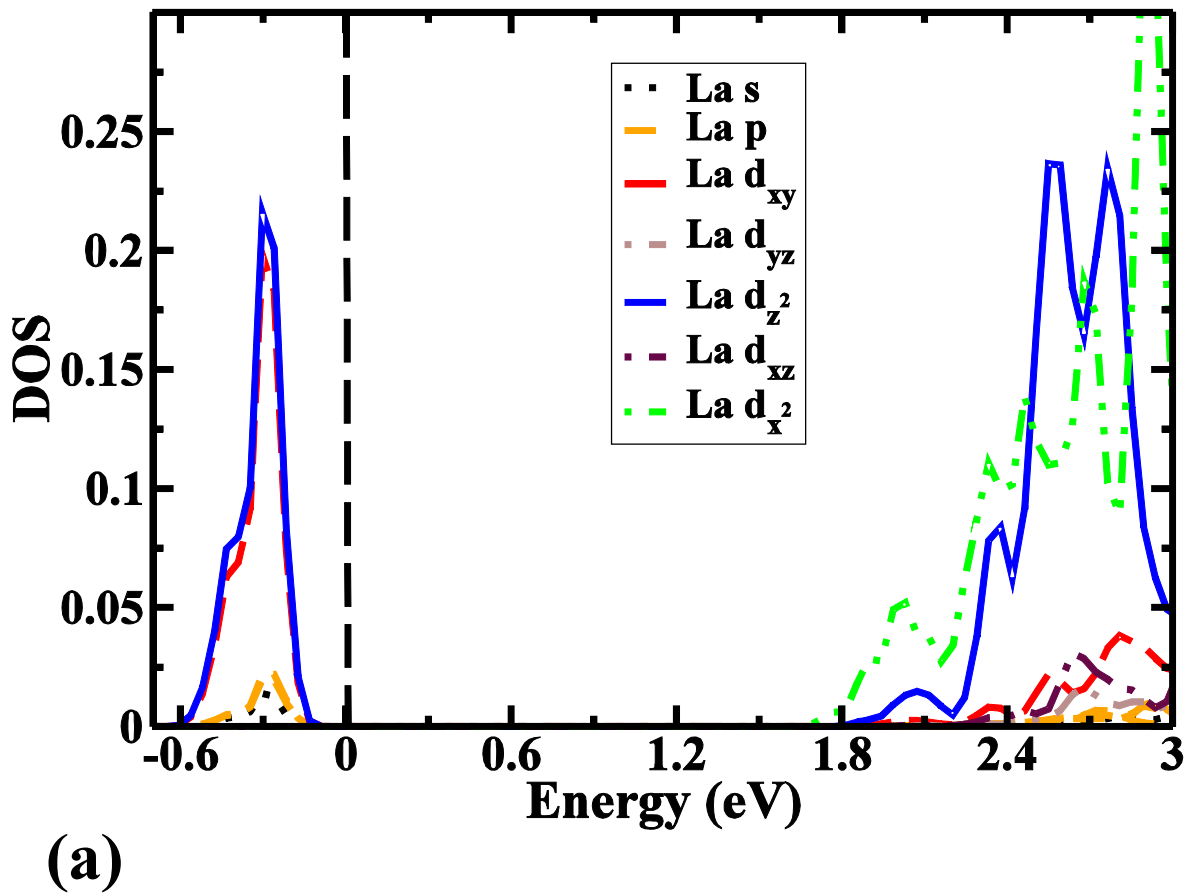

(a)

Figure 7a BL11919 19SEP2012

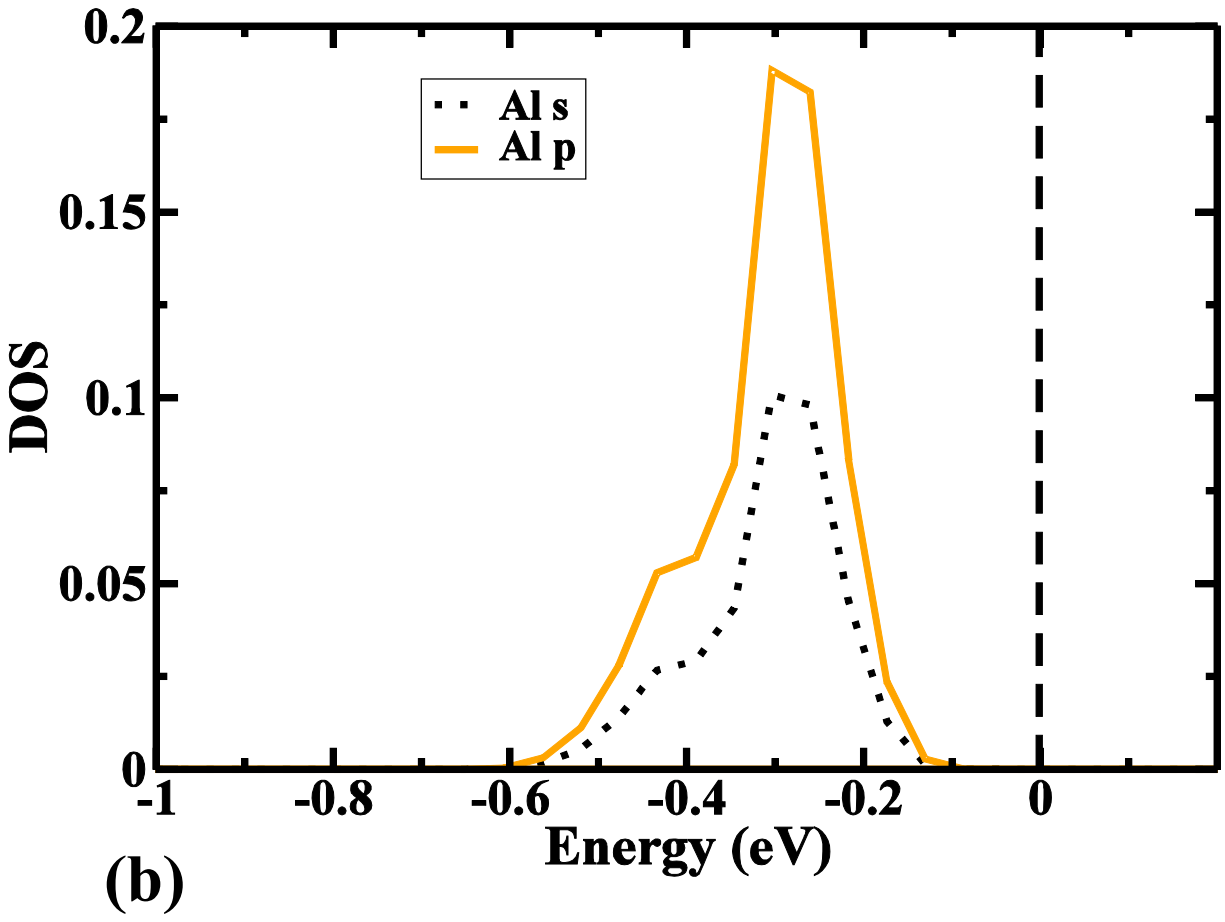

Figure 7b BL11919 19SEP2012

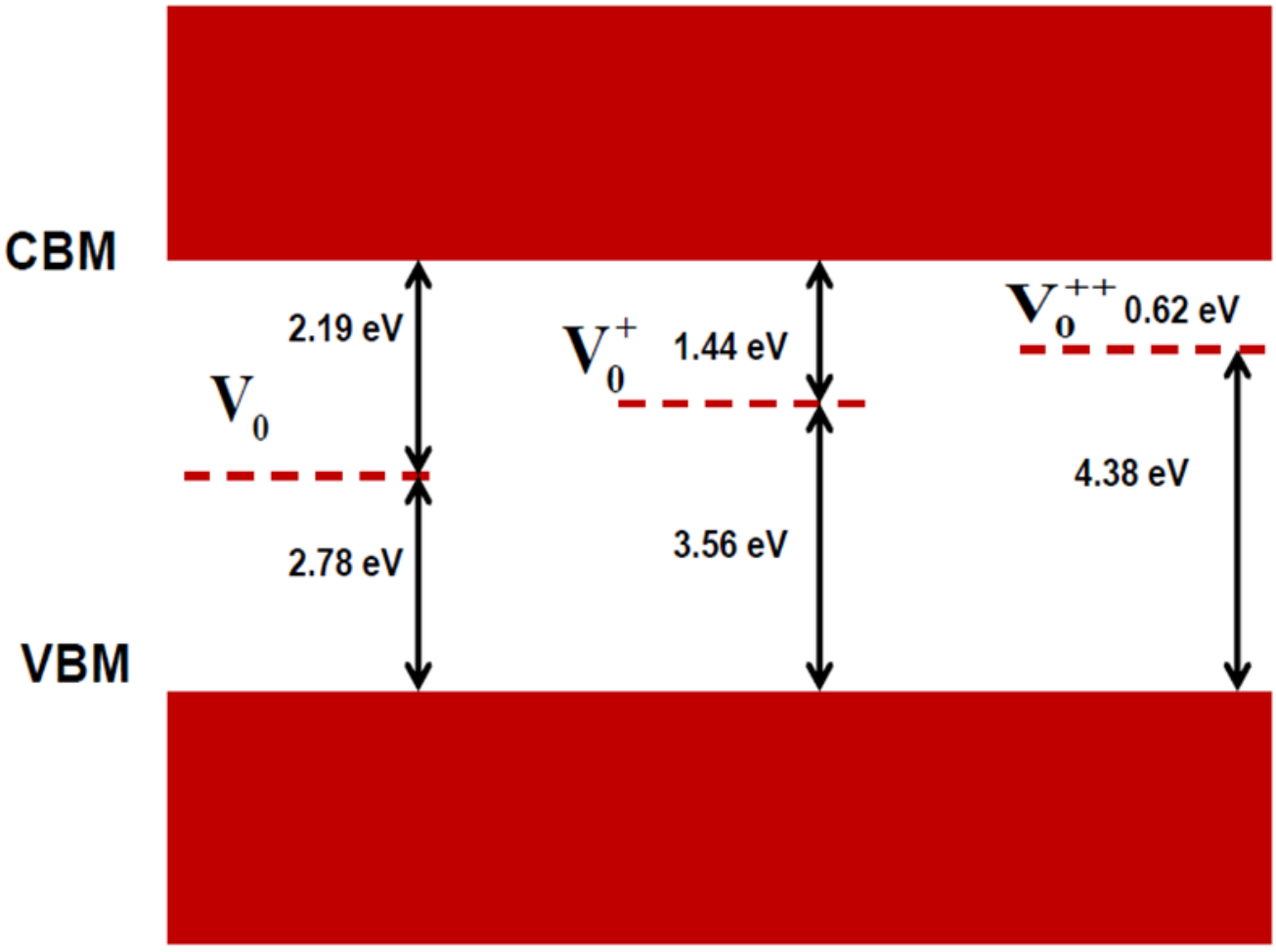

Figure 8 BL11919 19SEP2012

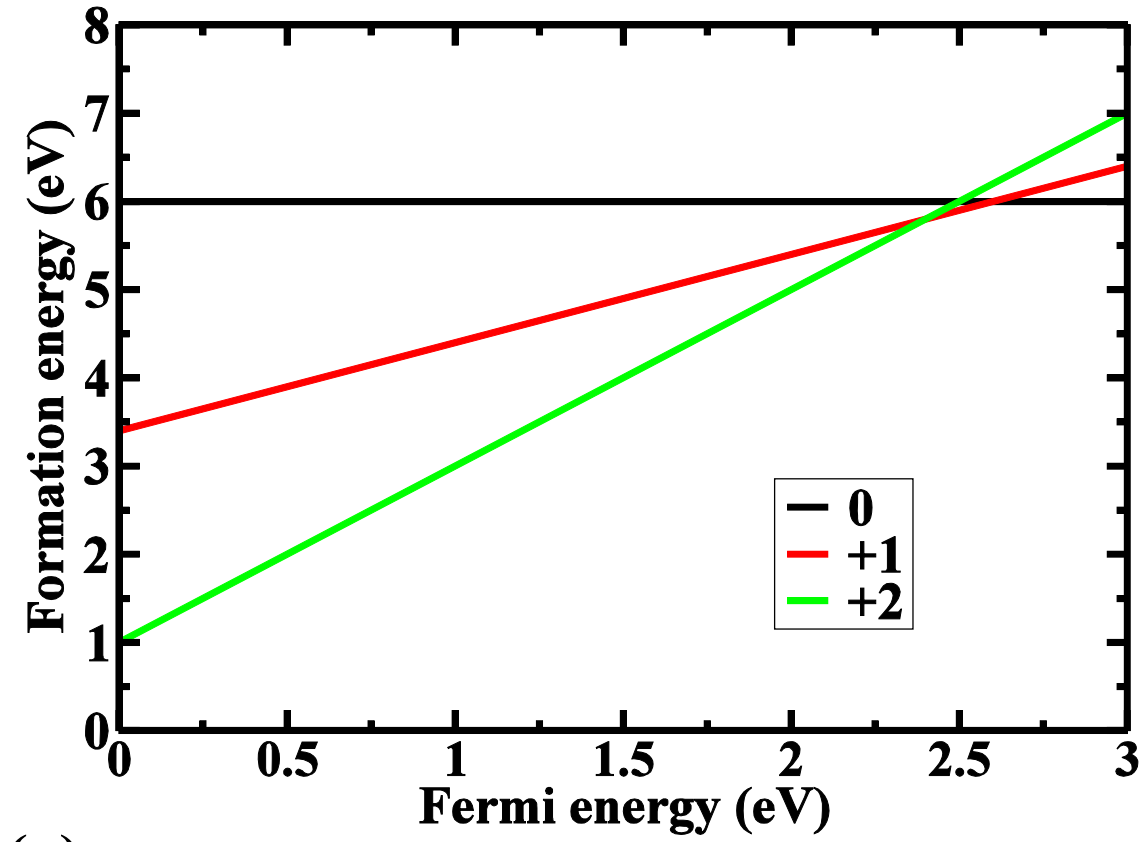

(a)

Figure 9a BL11919 19SEP2012

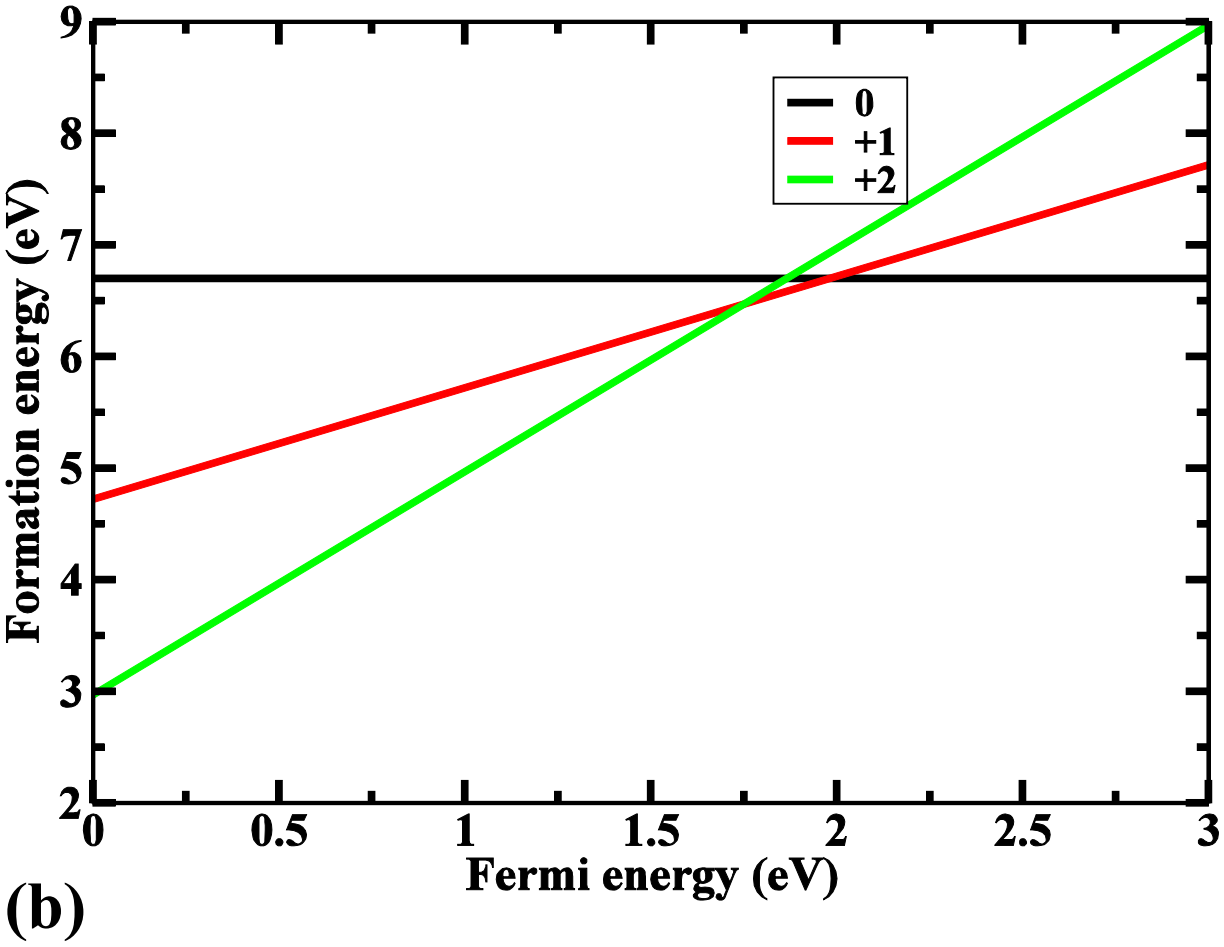

(b)

Figure 9b BL11919 19SEP2012

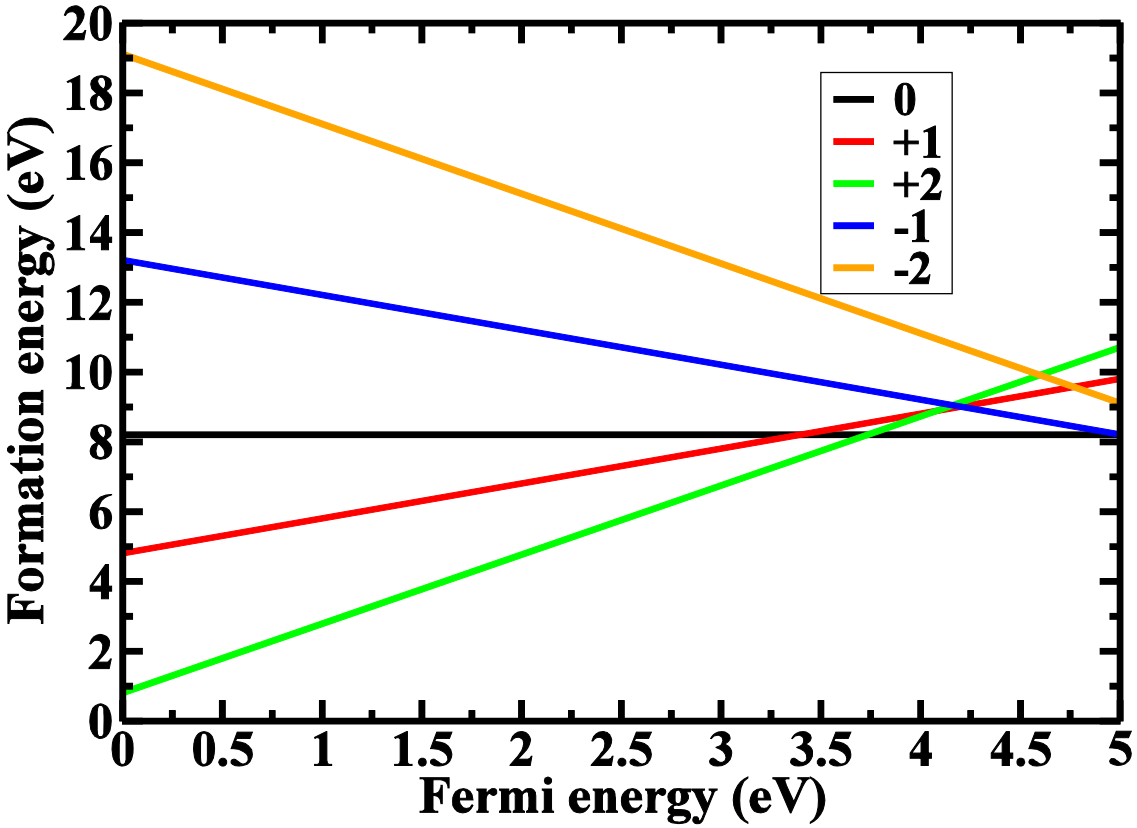

(a)

Figure 10a BL11919 19SEP2012

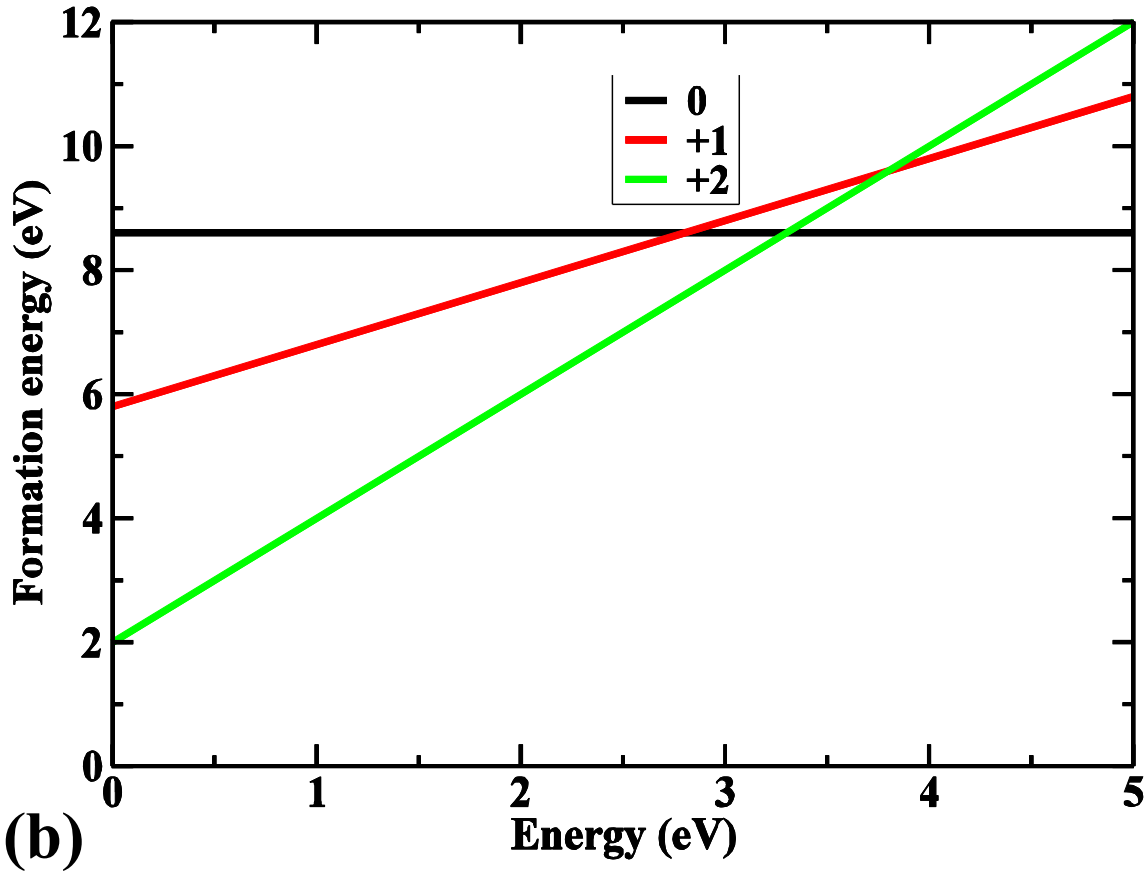

Figure 10b BL11919 19SEP2012

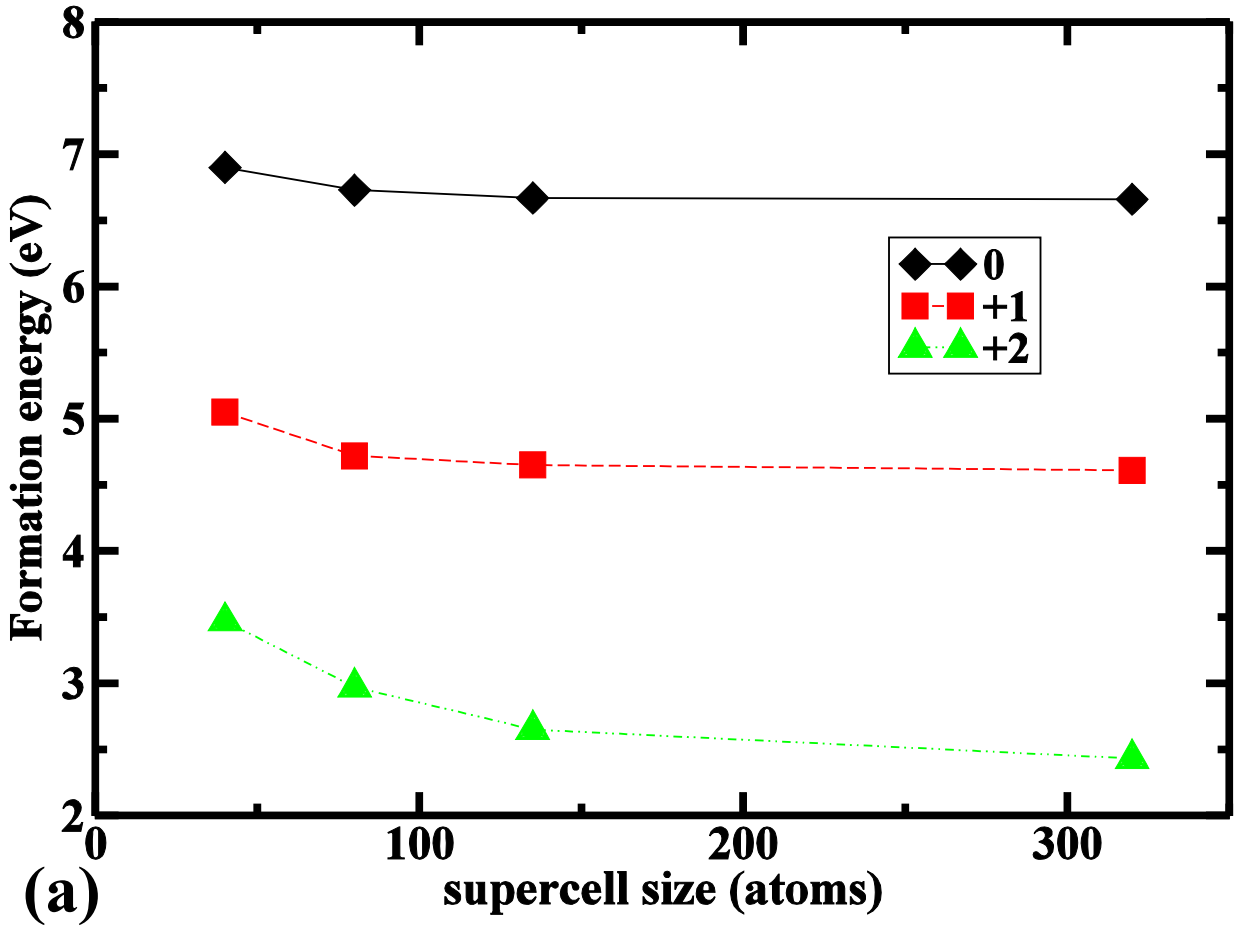

Figure 11a BL11919 19SEP2012

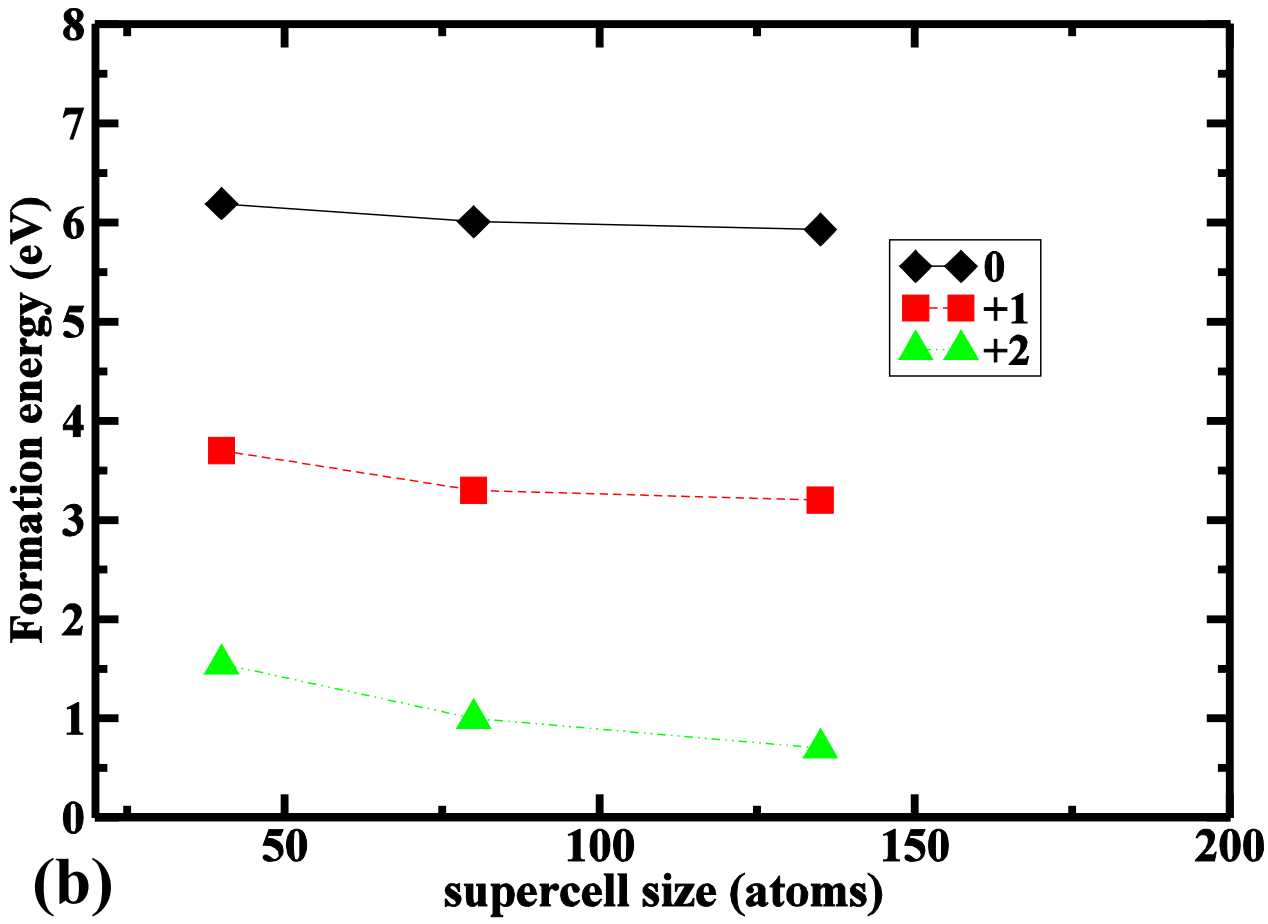

Figure 11b BL11919 19SEP2012